



Stabilization of air bubbles in oil by surfactant crystals: A route to produce air-in-oil foams and air-in-oil-in-water emulsions



Mathieu Brun^a, Mathieu Delamplé^a, Etienne Harte^b, Sophie Lecomte^b, Fernando Leal-Calderon^{b,*}

^a AGIR, 37, Avenue Albert Schweitzer, B.P. 100, 33402 Talence Cedex, France

^b Laboratoire Chimie et Biologie des Membranes et des Nanoobjets, Univ. Bordeaux, CBMN, UMR 5248, Allée Geoffroy St Hilaire, F-33600 Pessac, France

ARTICLE INFO

Article history:

Received 3 October 2014

Accepted 25 November 2014

Available online 3 December 2014

Keywords:

Nonaqueous foams

Air-in-oil-in-water emulsions

Crystallization

Stability

ABSTRACT

The incorporation of air in vegetable oils is highly sought after as it allows reducing the total fat content, while providing a light and pleasant texture. To meet consumers' requirements, nonaqueous foams must remain kinetically stable for several months and must withstand large deformations and flows. In this paper, we describe the fabrication of air-in-oil foams of outstanding stability, both at rest and under flow, based on the use of crystallizable surfactants (mixture of mono- and diglycerides). The air volume fraction is close to 55%, irrespective of the surfactant concentration. The air bubbles are protected against coalescence and Ostwald ripening by a dense layer of crystals. Moreover, the firmness of the surfactant crystal network formed in the oil bulk is large enough to hinder buoyancy driven phenomena. Finally, we demonstrate that the oil foams can be dispersed in an aqueous phase containing hydrocolloids to form a novel type of material: air-in-oil-in-water (A/O/W) emulsions.

© 2014 Elsevier Ltd. All rights reserved.

1. Introduction

Foams are dispersions of gas bubbles in a liquid containing surface-active species. The latter adsorb at the gas–liquid interface and are responsible both for the ability of a liquid to foam and for the stability of the resulting foams. The application range of foams is considerably widespread: it encompasses foods, cosmetics and personal care products, fire fighting, enhanced oil recovery, etc. Conventional foams stabilized by surfactant molecules generally exhibit short lifetime: from minutes to hours. In such systems, the kinetic evolution occurs through different mechanisms: Ostwald ripening, liquid drainage and bubble coalescence (Morrison & Ross, 2002; Prud'homme & Khan, 1996). Ostwald ripening is controlled by the solubility of the gas molecules in the liquid phase. The gas phase is transferred from small to large bubbles due to their different Laplace pressures. Coalescence consists of hole nucleation in the thin liquid film separating two bubbles in contact. If the hole reaches some critical size, it grows and the bubbles relax their shape under the effect of interfacial tension, providing a new drop with reduced surface area. The large density difference between the liquid phase and gas causes liquid to flow downwards through the network of Plateau borders. When the volume fraction of liquid in the dried foam becomes sufficiently small, films rupture and the foam is progressively destroyed.

Aqueous foams containing water as the continuous phase have been extensively studied (Exerowa & Kruglyakov, 1998). The most common

surface active-species used are foaming agents which are low molar mass surfactants, amphiphilic polymers or proteins. Recently, the use of solid particles as stabilizers of aqueous foams has been described, leading to foams which show no sign of either Ostwald ripening or coalescence over several months (Alargova, Warhadpande, Paunov, & Velev, 2004; Binks & Horozov, 2005; Fujii, Ryan, & Armes, 2006; Subramaniam, Mejean, Abkarian, & Stone, 2006). The irreversible anchoring of the particles at the air–water interfaces armors the bubbles and enhances their stability relative to foams stabilized by surface-active molecules. The same strategy is generally adopted in dairy technology for the stabilization of whipped creams or ice creams. In this case, partially crystallized droplets initially dispersed in the water phase adsorb and spread at the bubble/water interface (Hotrum, Cohen-Stuart, van Vliet, & van Aken, 2004) and form a rigid network in bulk entrapping the bubbles.

Nonaqueous foams have been less frequently studied, so far. In general, oil-continuous foams are difficult to obtain because the surface activity of surfactants in lipophilic solvents is much lower than in aqueous systems. The propensity of surfactants to adsorb at the oil–air interface is low because of the “hydrophobic” nature of the two immiscible media. However, several studies have shown that nonaqueous foams could be achieved from fluoroethylene particles (Binks, Rocher, & Kirkland, 2011), fluorinated clay platelet particles (Binks, Sekine, & Tyowua, 2014), or from liquid crystal dispersions (Friberg & Ahmad, 1971; Friberg, Blute, Kunieda, & Stenius, 1986; Friberg, Chang, Green, & Gilder, 1984). Monoglycerides form solid dispersions in organic solvents at room temperature and are efficient foam stabilizers (Shrestha, Aramaki, Kato, Takase, & Kunieda, 2006; Shrestha, Sato, et al., 2006). Their unique properties for the stabilization of nonaqueous

* Corresponding author at: Laboratoire CBMN (UMR CNRS 5248), Bat. B14, Allée Geoffroy Saint Hilaire, 33600 Pessac, France. Tel.: +33 5 40 00 68 38.

E-mail address: fleal@enscbp.fr (F. Leal-Calderon).

foams mainly rely on their surface activity and on their high melting point, allowing the formation of crystals at room temperature when mixed with oils (Shrestha, Aramaki, et al., 2006). The shelf life of the nonaqueous foams observed with these solid dispersions varies from minutes to hours depending on the shape, size and concentration of the solid particles (Shrestha, Aramaki, et al., 2006). Similarly, Kunieda et al. (2007) obtained nonaqueous foams with diglycerides surfactants in organic solvents such as liquid paraffin, or squalene and the foaming properties have been described by the phase behavior (Shrestha, Kaneko, et al., 2006). Shrestha, Shrestha, Sharma, and Aramaki (2008) studied the nonaqueous foaming properties of diglycerol monolaurate in olive oil and it was found that lamellar liquid crystal particles could also stabilize nonaqueous foams for minutes to several hours depending on the concentration and the size of the dispersed particles. The study was extended to diglycerol monopalmitate and foams with outstanding stability (more than one month) were successfully obtained (Shrestha, Shrestha, Solans, Gonzalez, & Aramaki, 2010).

Following the seminal work of Shrestha, Aramaki, et al. (2006), Shrestha, Kaneko, et al. (2006), Shrestha, Sato, et al. (2006), Shrestha et al. (2008, 2010), in the present study, we used a food grade surfactant mixture of long-chain mono and diglycerides (E471) to elaborate highly stable foams in rapeseed oil. Such materials may be very useful for practical applications such as shaving creams, whipped creams, and toppings. Our strategy aims at using the surfactant crystal network to stabilize air bubbles by forming a rigid layer at their interface and a rigid network in the oil bulk. The overrun is measured and the stability of the obtained nonaqueous foams is assessed both at rest and under flow. We also probe the ability of the obtained foams to be emulsified in an aqueous phase containing food hydrocolloids to produce novel edible materials of the air-in-oil-in-water type. Our approach paves the way to the formulation of food products with reduced caloric content.

2. Materials and methods

2.1. Materials

The oil phase used for the formulations was rapeseed oil (density at 20 °C = 0.92 g cm⁻³, viscosity = 80 cP) from Maurel (France). The lipophilic surfactant was Lamemul® K 2000 K, hereafter referred to as MDG (mono and diglycerides), purchased from BASF. It consists of distilled mono and diglycerides of edible saturated fatty acids, vegetable based, and spray chilled to obtain fine particles. Its total content in monoglycerides is larger than 90 wt.% and it exhibits a melting range between 50 and 78 °C. Emulsions were formulated using sodium caseinate ($M_w \approx 20\,000\text{ g}\cdot\text{mol}^{-1}$) (Lactoprot, Germany) or gum arabic from (CNI, France), as the hydrophilic emulsifier, and hydroxyethyl cellulose (Fluka, France) or Xanthan Keltrol® (Kelco Inc., U.S.), as thickening/gelling agent. Sodium azide (NaN₃) was used as a biocide and was purchased from Merck. All species were used as received. The water used in the experiments was deionized with a resistivity close to 15 MΩ·cm at 20 °C.

2.2. Preparation of MDG/rapeseed oil mixtures

Several mixtures whose MDG concentration ranged from 2.5 to 20 wt.% were prepared by dissolving MDG in powder form into rapeseed oil warmed at 80 °C. Transparent solutions were obtained at this temperature. The samples were then stored at 20 °C and became turbid upon cooling because of the formation of MDG crystals.

2.3. Differential scanning calorimetry (DSC) experiments

We used DSC as an indirect way to assess the crystallization extent of MDG/rapeseed oil mixtures. Thermal analyses were conducted on a differential scanning calorimeter (Setaram, model micro DSC VII) in aluminum pans of 0.7 ml hermetically sealed. A hermetically sealed

aluminum pan containing rapeseed oil was used as reference. Calibration was made with water (melting point = 0 °C, melting enthalpy = $\Delta H_m = 333\text{ J}\cdot\text{g}^{-1}$), decane (melting point = -27.3 °C, $\Delta H_m = 11.6\text{ J}\cdot\text{g}^{-1}$) and naphthalene (melting point = 80.3 °C, $\Delta H_m = 145.9\text{ J}\cdot\text{g}^{-1}$) at three different rates (0.1, 0.5 and 1 °C·min⁻¹). Most of the DSC experiments were carried out from 20 to 90 °C (melting curves) at a rate of +1 °C·min⁻¹.

2.4. Controlled shear experiments

Some samples (MDG/oil mixtures, oil foams, emulsions) were submitted to a controlled shear by means of a Couette's cell (concentric cylinders geometry, Ademtech SA, France). A detailed scheme of the setup can be found in Mabile et al. (2000). Approximately 50 ml of sample was loaded in the injection chamber and was syringed in the interspace separating the rotor and the stator. The inner cylinder of radius $R \approx 20\text{ mm}$ is moved by a motor that rotates at a selected angular velocity, ω , which can reach up to 71.2 rad·s⁻¹. The outer cylinder is immobile, and the gap between the stator and the rotor is fixed either at $e = 100$ or 200 μm. For the maximum angular velocity, and $e = 100\text{ μm}$, we are able to reach very high shear rates, $\dot{\gamma} \approx R\omega/e \approx 14,200\text{ s}^{-1}$, in simple shear flow conditions. The injection rate was adapted so that the residence time in the gap was of the order of 5 s. Under such conditions, warming of the sample was negligible and the temperature of the systems at the exit of the cell was very close to room temperature (~20 °C).

2.5. Whipping process and measurement of the overrun

Foams were obtained by introducing the MDG/oil mixture at room temperature into the bowl of a Kitchen Aid blender (model 5KSM150PS EER) equipped with a wire whisk. The samples were agitated for 15 min at a constant rotation rate (level 10 on a scale from 1 to 10) in order to incorporate air bubbles into the oil phase. Some foams were further processed in the Couette's cell to reduce the bubble size.

We define the overrun as the volume percentage of air incorporated into the oil foam:

$$\theta = \frac{V_{air}}{V_{air} + V_{oil}} \quad (1)$$

where V_{air} and V_{oil} are the volumes of air and of the oil phase (MDG + rapeseed oil) in the foam, respectively. The foams were introduced in glass tubes of 1 cm in diameter and 10 cm high. The overrun was estimated by measuring the volume difference as the sample was warmed from room temperature to 80 °C. Indeed, at room temperature, the foam contained air bubbles entrapped in the crystal network and its volume was equal to $V_{air} + V_{oil}$. At 80 °C, MDG crystals were fully molten resulting in rapid destabilization of the foam, so that the final volume was V_{oil} . The overrun was then straightforwardly obtained using Eq. (1).

2.6. Fabrication of air-in-oil-in-water emulsions

An aqueous phase containing an emulsifier (gum arabic or sodium caseinate), a thickener (hydroxyethyl cellulose or xanthan) and sodium azide was first prepared. The exact composition will be provided in Section 3.3. Foams were then progressively incorporated in the aqueous phase under manual stirring, at room temperature. The obtained coarse dispersion was finally sheared in the Couette's cell to reduce the droplet size.

2.7. Microscope observations

An Olympus BX51 (Zeiss, Germany) phase contrast microscope equipped with a digital camera was used to take photomicrographs of the MDG/oil mixtures, foams and emulsions. A small amount of sample was taken on the microscope slide and mounted by a thin cover slip. The

samples were viewed through the microscope to observe the shape and size of the dispersed objects. When necessary, a cross-polarizing configuration of the microscope was adopted to visualize the MDG crystals dispersed in the oil phase.

Foams were also analyzed by Raman confocal microscopy. A small amount of sample was carefully deposited in between the microscope slides. Raman spectra were recorded using a WITec (Ulm, Germany) Alpha300RS confocal Raman microscope. The excitation wavelength of 532 nm was provided by a frequency-doubled Nd:YAG laser. The beam was focused on the sample using an Olympus (100 \times /0.95 NA) objective, and the power at the sample was close to 10 mW. The sample was located on a piezoelectrically driven microscope scanning stage, with a x–y-resolution of 5 nm, and a z-resolution of 2 nm. The integration time for each spectrum was 36 ms. A Raman spectrum was recorded every 400 nm along the x and y directions. Each image resulted in about 2500 (50 \times 50) spectra, (20 \times 20) 400 μm^2 and 90 s acquisition time.

The average bubble size in foams and the average droplet in emulsions were determined by direct imaging. The images were recorded and the dimensions of about 50 bubbles or droplets were measured. Hereafter, the sizes are provided as number-averaged values.

2.8. Surface tension measurements

The pendant drop method was used to measure the surface tension of the oil phase at 20 °C. This technique involves the determination of the profile of a droplet of one denser liquid (oil phase) suspended in another fluid (air in this case). The balance between gravity and surface forces determines the profile of the drop. The images of the drop are taken at regular time intervals with the aid of a video frame grabber of a digital camera. The digital signals are analyzed considering Laplace's equation to determine the interfacial tension from the drop profile. The apparatus used in the present study was KSV's CAM200 (Sodexim SA, France).

2.9. Rheological measurements

Both steady flow and oscillatory experiments were performed at 20 °C with an ARG2 rheometer (TA instruments) on MDG/oil mixtures and on oil foams. Oscillatory experiments were conducted in the linear

regime, at a deformation amplitude of 0.2%, and at a frequency of 1 Hz. We adopted a parallel-plate geometry with a gap of 1 mm and rough surfaces in order to avoid wall slipping. Despite the fact that the applied stress was not constant over the whole sheared volume, parallel plate geometry was preferred in order to avoid problems related to confinement. Generally foams are fragile and consequently we took all possible precautions in order to preserve their integrity during the loading process to obtain reproducible data. The oil foams were placed in the cell of the rheometer very carefully; the sample compression during loading was the minimal possible and was always done at the smallest rate. Temperature within the sample was controlled with a precision of 0.1 °C via a thermoelectric Peltier module. All rheological measurements were conducted in triplicate and the deviation between experiments never exceeded 20%.

3. Results and discussion

3.1. Behavior of the MDG/oil mixture

We first consider the behavior of MDG/oil mixtures. The mixtures were prepared at 80 °C and upon cooling, MDG formed crystals that provided an opaque aspect. Fig. 1 shows both the macroscopic and the microscopic appearances of a 10 wt.% MDG mixture after 24-hour storage at room temperature. The obtained sample is a very viscous paste with a matt surface (Fig. 1-a). Microscope observations under cross-polarizing conditions reveal bright spots indicating the presence of large crystals whose size is of the order of several hundreds of micrometers (Fig. 1-b). In industrial pilots, crystallization may occur at rest, such as in a cooling tunnel, or instead occur under conditions of high shear, such as in a scraped surface heat exchanger. To limit the energy cost associated to fluid transportation, it is important to reduce the viscosity as much as possible. After a storage period of 24 h at 20 °C, the paste was processed in the Couette's cell at a shear rate of 1000 s^{-1} with a gap $e = 200 \mu\text{m}$ in order to reduce the crystal size and to improve its handleability. Fig. 1-c shows the macroscopic aspect of the resulting material. The evolution of the sample whiteness and the glassy aspect of the surface suggest that the sample submitted to shear has undergone a significant structural change. This is confirmed by the microscope image of Fig. 1-d where it can be seen that crystals are poorly

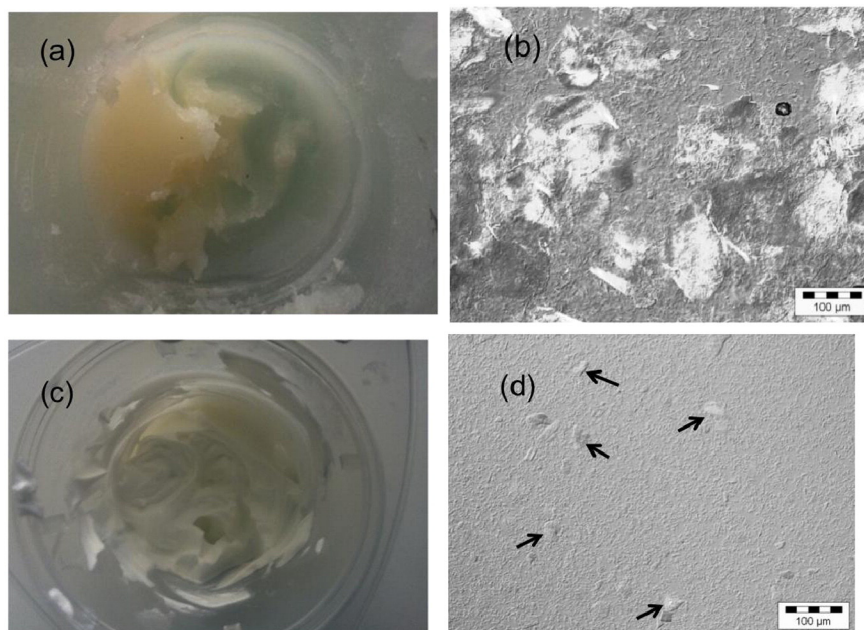


Fig. 1. Aspect of a MDG/oil mixture before and after being sheared in the Couette's cell at 1000 s^{-1} . The MDG content in the oil phase is 10 wt.%. (a): Unsheared, macroscopic view; (b) unsheared; microscopic view; (c): sheared; macroscopic view; (d): sheared; microscopic view.

Table 1
Rheological properties of the MDG/oil mixtures before and after shear application in the Couette's cell at 1000 s^{-1} .

MDG content in the oil phase (wt.%)	Before shear application			After shear application		
	G' (Pa)	G'' (Pa)	η (Pa·s)	G' (Pa)	G'' (Pa)	η (Pa·s)
2.5	$(9.4 \pm 0.5) \times 10^2$	$(4.6 \pm 0.3) \times 10^2$	4.8 ± 0.3	$(4.3 \pm 0.3) \times 10^2$	$(1.1 \pm 0.1) \times 10^2$	1.1 ± 0.1
5.0	$(2.0 \pm 0.1) \times 10^3$	$(6.2 \pm 0.3) \times 10^2$	11.6 ± 0.6	$(8.2 \pm 0.4) \times 10^2$	$(2.4 \pm 0.1) \times 10^2$	3.2 ± 0.2
10.0	$(5.2 \pm 0.3) \times 10^4$	$(1.7 \pm 0.2) \times 10^4$	34.8 ± 1.5	$(1.1 \pm 0.1) \times 10^3$	$(4.5 \pm 0.3) \times 10^2$	11.7 ± 0.6
15.0	$(2.5 \pm 0.1) \times 10^5$	$(1.3 \pm 0.1) \times 10^5$	74.1 ± 3.7	$(3.1 \pm 0.2) \times 10^3$	$(1.3 \pm 0.1) \times 10^3$	36.3 ± 2.0
20.0	$(3.9 \pm 0.2) \times 10^5$	$(2.3 \pm 0.2) \times 10^5$	101.7 ± 5.0	$(6.5 \pm 0.3) \times 10^3$	$(2.8 \pm 0.2) \times 10^3$	75.2 ± 3.5

refracting compared with those in Fig. 1-b, reflecting their much smaller size. Some crystals indicated by the arrows are large enough to be discernible but their size is smaller than $40 \mu\text{m}$.

The evolution of the crystal size has profound consequences for the rheological properties of the paste. In Table 1, we report the values of the viscoelastic moduli, G' , G'' , and of the viscosity measured at 10 s^{-1} (measured following the methods described in Section 2.9) before and after shear application. The laminar shear applied in the Couette's cell reduces the gel strength (G' and G'') in the low deformation regime as well as the viscosity of the paste under steady flow conditions. The general scenario for fat crystallization is first nucleation and growth of crystals, followed by their aggregation and partial coalescence due Van der Waals attraction ending up with the formation of a crystalline 3D-network (Walstra, Kloek, & van Vliet, 2001). It can be argued that the shear has provoked particle fragmentation (break-up) and has also reduced particle roughness.

DSC measurements were carried out in order to characterize the melting range of MDG in the mixtures. Once sheared, the binary mixtures were stored at room temperature for 24 h before being submitted to a temperature ramp from 20 to $90 \text{ }^\circ\text{C}$ at $+1 \text{ }^\circ\text{C} \cdot \text{min}^{-1}$. Fig. 2 shows the melting thermograms obtained at different MDG fractions from 2.5 to 20 wt.%. All thermograms exhibit the same shape. However, the temperature at the peak (i.e. maximum heat flow) shifts towards higher temperatures as the MDG content increases probably due to the effect of the mixing entropy (Yuqing Zhou & Hartel, 2006).

3.2. MDG/oil foams

Foams were obtained following the whipping process described in Section 2.5. The starting material was a binary MDG/oil mixture stored for 24 h at room temperature and processed in the Couette's cell. The incorporation of air was evidenced by warming the samples at $80 \text{ }^\circ\text{C}$. In the molten state, MDG molecules were poor stabilizers and the foam

collapsed within a few minutes. This is illustrated in Fig. 3 where the initial foam transforms into a transparent oil solution whose volume is significantly smaller than that of the foam. Such instability leading to full release of the air was exploited to measure the overrun following the method explained in Section 2.5. The obtained values are plotted in Fig. 4 as a function of the MDG content. Within experimental uncertainty, it can be stated that the overrun is roughly constant and is of the order of 55 vol.%. This value is close to the random close packing fraction of monodisperse spheres (64 vol.%) above which randomly distributed spheres are compressed against each other because of the packing constraints. It is thus likely that the bubbles coalesce and are expelled from the foam at high volume fractions ($> 55\%$) where bubbles are forced to be in permanent contact.

For $\phi_{\text{MDG}} \geq 5 \text{ wt.}\%$, the foams remained apparently homogenous and their air fraction did not evolve for more than 1 month. Indeed, they were stored at room temperature and their volume remained constant reflecting the retention of air bubbles over that time period. Only the foam with $\phi_{\text{MDG}} = 2.5 \text{ wt.}\%$ underwent partial phase separation with a fraction of oil residing at the bottom of the vessel (see Fig. 5). In this sample, the firmness of the crystal network is insufficient to maintain the initial colloidal structure. The bottom phase is transparent, meaning that this part of the sample is devoid of MDG crystals. It can be hypothesized that crystals are anchored to the bubbles which tend to be dragged towards the top of the vessel under the effect of the buoyant stress. Fig. 6 shows 2 images of a foam with $\phi_{\text{MDG}} = 10 \text{ wt.}\%$, taken in a 3-month interval using conventional transmission microscopy. Bubbles appear as bright spots surrounded by a dark thick shell because of the large refractive index mismatch between oil and air. As can be seen, the diameter of the bubbles is the range from 10 to $50 \mu\text{m}$ and the distribution does not undergo any noticeable evolution over time. It is worth noticing that the same characteristic bubble size was obtained, whatever the MDG content in the oil phase. One plausible explanation for the absence of aging phenomena like coalescence and

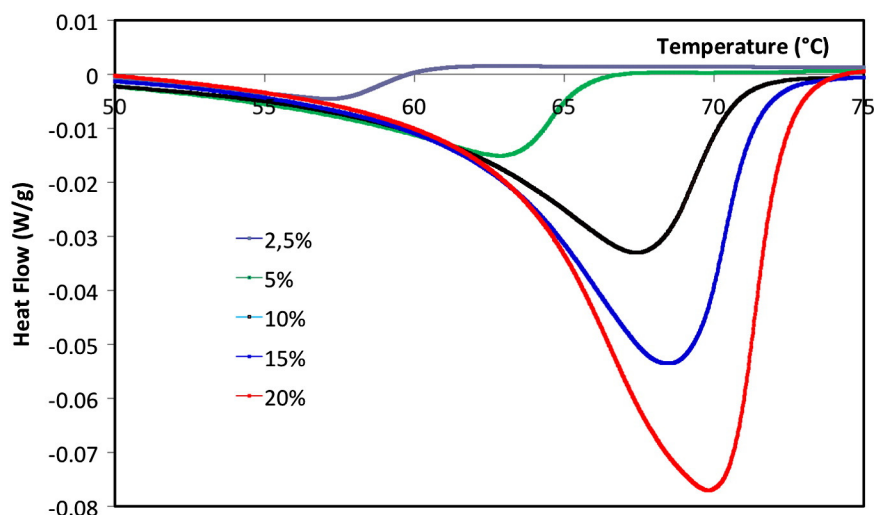


Fig. 2. Melting thermograms of MDG/paraffin oil mixtures obtained at different MDG fractions from 2.5 to 100 wt.%.

Ostwald ripening is that the interfaces are covered by a dense layer of irreversibly adsorbed crystals. Both coalescence and Ostwald ripening produce a continuous increase of the average bubble size and thus a reduction of the air–oil interface. As the bubble area decreases, the irreversibly adsorbed crystal would not be released and so the aging phenomena would be mechanically hindered. In Fig. 6, it can be noticed that some bubbles are not spherical. Again, this observation could reflect the fact that the interfaces are mechanically rigid owing to the presence of adsorbed crystals.

Ostwald ripening is characterized by either a constant volume rate ω_3 (diffusion controlled ripening), or a constant surface rate ω_2 (surface-controlled ripening) depending on the origin of the transfer mechanism:

$$\frac{d\langle r \rangle^\alpha}{dt} = \omega_\alpha \quad (\alpha = 2, 3) \quad (2)$$

where $\langle r \rangle$ is the average radius. If ripening is controlled by diffusion across the continuous phase, then the cube of the radius increases linearly with time ($\alpha = 3$) and the ripening rate can be derived using the Lifshitz and Slyozov theory (Lifshitz & Slyozov, 1961; Wagner, 1961):

$$\omega_3 = \frac{d\langle r \rangle^3}{dt} = \frac{8}{9} \left[\frac{S\gamma V_m D}{R_g T} \right] \quad (3)$$

where γ is the surface tension, R_g is the molar gas constant, T is the absolute temperature, V_m is the molar volume of the diffusing species, S and D are the solubility and the diffusion coefficient of the diffusing molecules in the continuous phase. Data about the solubility of nitrogen, the main component of air, in various fluids are available in Battino, Rettich, and Tominaga (1984). The value measured at 20 °C expressed as a mole fraction at 0.1 MPa partial pressure of gas is equal to 2.81×10^{-3} in olive oil. Although the oil used in this study was not olive oil, the previous value can be taken as being representative of triglyceride oils. The diffusion coefficient, D , was estimated considering Einstein equation:

$$D = \frac{kT}{6\pi\eta_{oil}a} \quad (4)$$

where k is the Maxwell–Boltzmann constant, η_{oil} is the viscosity of the liquid oil phase (≈ 80 cP) and a is the molecular radius of the gas (≈ 1.5 Å for N_2). The equilibrium surface tension of rapeseed oil and

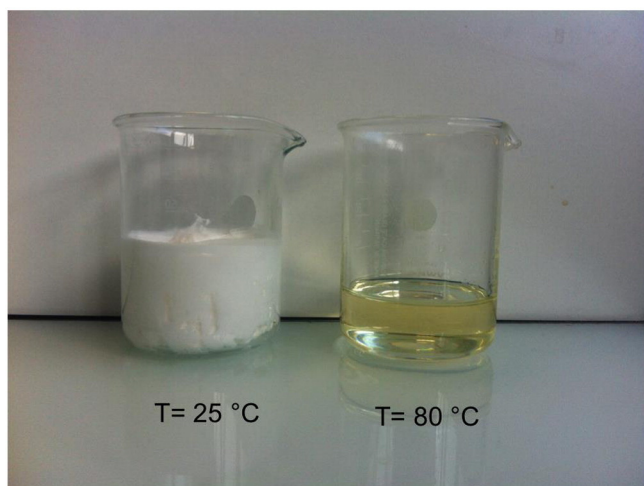


Fig. 3. Images showing foam destabilization as the temperature is raised from 20 to 80 °C. The MDG content in the oil phase is 10 wt.%. The same mass of foam was introduced in the two beakers. The right hand size beaker was warmed at 80 °C in an oven and immediately deposited on the bench prior to MDG recrystallization.

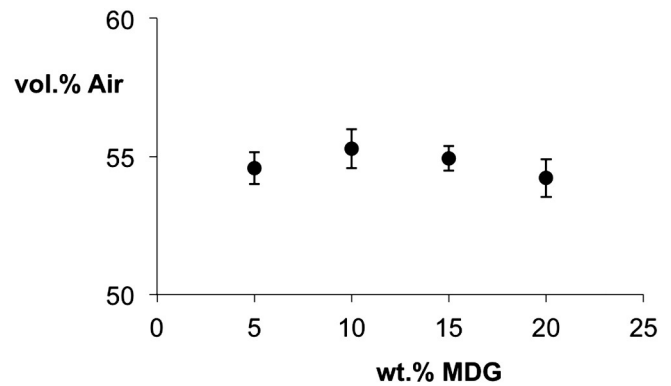


Fig. 4. Overrun (vol.% air) on the foams as a function of the MDG content in the oil phase.

the crystal dispersion as a function of surfactant concentrations were measured at 20 °C. Rapeseed has a surface tension value of $33.8 \text{ mN}\cdot\text{m}^{-1}$ and the addition of MDG (0.25–0.5 wt.%) reduces the value to $29.5 \text{ mN}\cdot\text{m}^{-1}$. Eq. (3) is in principle valid in the limit of very dilute systems. In general, it is expected that foams with higher volume fractions of the disperse phase will have broader particle size distributions and faster absolute growth rates than those predicted by the Lifshitz and Slyozov model. The theoretical rate of ripening must therefore be corrected by a factor $f(\phi)$ that reflects the dependence of the coarsening rate on the dispersed phase volume fraction ϕ . Following the mean field model of Lemlich (1978), $f(\phi) = 4.7\phi / (1 - \phi)$. Considering the previous data, it is possible to evaluate the ripening rate and the obtained value is $\omega_3 \approx 5 \times 10^{-25} \text{ m}^3\cdot\text{s}^{-1}$. Thus, after a three-month storage, the increment in $\langle r \rangle$ is only $1.5 \mu\text{m}$, which is negligible considering that the initial average bubble radius is close to $25 \mu\text{m}$. In very concentrated foams ($\phi > 95\%$), air bubbles are highly compressed and exhibit flat facet at each contact. In this limit, Ostwald ripening is surface controlled (Durian, Weitz, & Pine, 1991) and the variation of the average radius occurs at rates that are one to several orders of magnitude larger than in diffusion controlled ripening. It is likely that a fraction of bubbles is in permanent contact in our foams. However, the apparent invariance of the size distribution after several months (see Fig. 6) pleads in favor of the formation of a dense crystal layer around the bubbles that considerably reduces gas permeability across the thin liquid films.

At temperatures above 78 °C, foam destruction occurs at a very fast rate (within minutes) indicating that MDG molecules are very poor stabilizers in the molten state and that crystals are ensuring stability against coalescence at a low temperature. To demonstrate that crystals are actually present at the interface, a foam was deposited in between two transparent microscope slides and warmed at 80 °C. The air bubbles rapidly coalesced forming very large cells visible to the naked eye. Then, the evolution scenario upon cooling was recorded under the microscope. Fig. 7-a corresponds to a very early stage of the crystallization

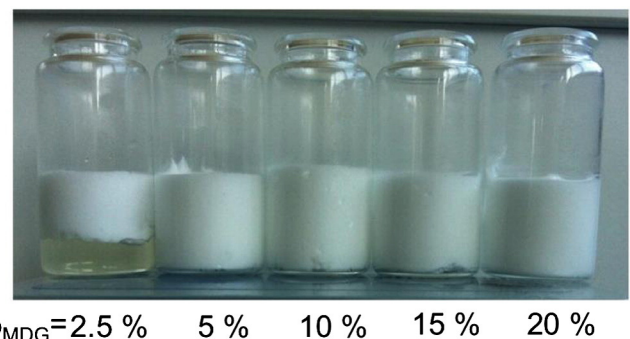


Fig. 5. Aspect of the foams after one-month storage.

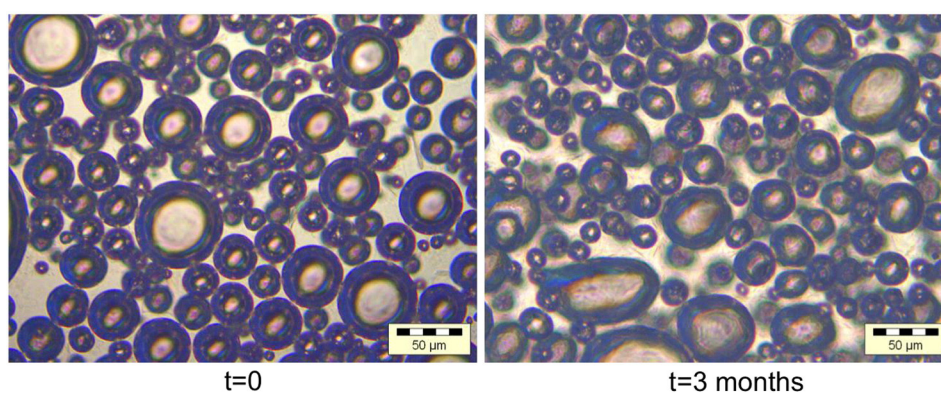


Fig. 6. Microscope images of the same foam taken in a one-month interval. The MDG content in the oil phase is 10 wt.%.

process. The microscope is focused at the equatorial plane of a large air bubble. Fig. 7-b was taken at the same location but at a more advanced stage of crystallization. It clearly appears that crystals are protruding into the air phase and seem to form a dense compact layer. We are aware that this configuration is not the same as in whipping experiments where air bubbles are incorporated in a matrix containing already formed crystals. However, this simple experiment demonstrates that crystals exhibit some affinity for the air–oil interface.

Confocal Raman microscopy was carried out to obtain a chemical image of the sample and then discern the preferential location of MDG crystals. Fig. 8 shows an optical image of the sample under white light illumination about 24 h after sample preparation. The surface of the air cells is wrinkled as a result of the adsorption of fat crystals. The frame indicates the area of the Raman mapping. First, the Raman spectra of rapeseed oil and MDG were separately recorded on bulk materials (see Supporting information 1). Specific bands for each compound were determined. The Raman spectrum of rapeseed oil reveals the presence of unsaturated fatty acid chains. The $\nu_{\text{C}=\text{C}}$ and the $\nu_{\text{C}-\text{H}}$ stretching vibrations are observed at 1665 cm^{-1} and 3010 cm^{-1} , respectively. These two bands are not present on the Raman spectrum of MDG that mostly contains saturated chains. To perform Raman imaging, we selected specific bands for each compound. The 1655 cm^{-1} band was used to identify rapeseed oil and the 1069 , 1134 and 2887 cm^{-1} bands were selected for the characterization of MDG. At each pixel, these bands were integrated after baseline subtraction. The integration of the band at 1665 cm^{-1} gives an image indicating the presence of rapeseed oil in the analyzed surface. For the detection of MDG material, three sets of images were obtained from the integration

of the 3 bands at 1069 , 1134 and 2887 cm^{-1} . The multiplication of these three images gave one image showing the presence of MDG with an improved signal to noise ratio. Fig. 9-a and b displays the corresponding Raman intensity images allowing both MDG and oil localization. Fig. 9-c corresponds to the superposition of the previous images using a color-coded format: red for MDG, green for oil and black for air bubbles. We clearly observe the presence of MDG crystals in bulk as large aggregates but also at the oil/air interface. Owing to its important thickness ($\sim 1\text{ }\mu\text{m}$), the interfacial crystal layer may contribute to the outstanding stability of the foams against coalescence and Ostwald ripening.

The foams retained their colloidal structure during prolonged storage and oil leakage at the bottom of the samples was not discernable after 3 months, except for the foam with $\phi_{\text{MDG}} = 2.5\text{ wt.}\%$. Air bubbles are thus trapped in the gel network formed by MDG crystals. Its firmness is sufficient to avoid gravity driven phenomena like bubble rising and oil drainage that would decrease the liquid fraction at the top of the foams and would accelerate destruction phenomena. An important feature of these materials is their rheological behavior: they exhibit considerable yield stress and viscoelastic properties. The viscoelastic moduli G' and G'' , and the yield stress, τ_v , of foams were measured and are reported in Table 2. The storage modulus, G' , is larger than the viscous one, G'' , reflecting the essentially elastic nature of the material. Interestingly, the moduli of the foams are larger than those of the corresponding oil/MDG mixture they are deriving from. This result reflects the impact of air bubbles, especially the mechanical properties of the rigid layers formed by the solid particles at the oil–air interface (Arditty, Schmitt, & Leal-Calderon, 2005). A recipient containing

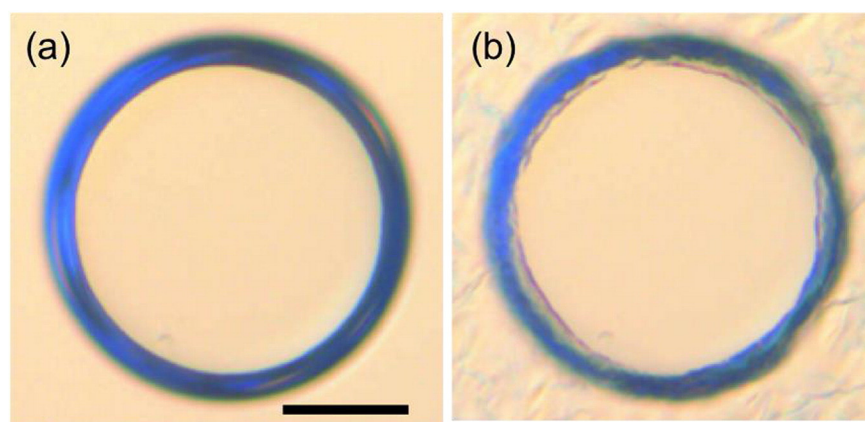


Fig. 7. Microscope images showing the evolution of the crystallization process as temperature decreases from 80 to $20\text{ }^{\circ}\text{C}$. The microscope is focused on the equatorial plane of a large air bubble. Panel (a) corresponds to a very early stage of the crystallization process. Panel (b) was taken at the same location but at a more advanced stage of crystallization. The MDG content in the oil phase is $10\text{ wt.}\%$. The bar corresponds to $100\text{ }\mu\text{m}$.

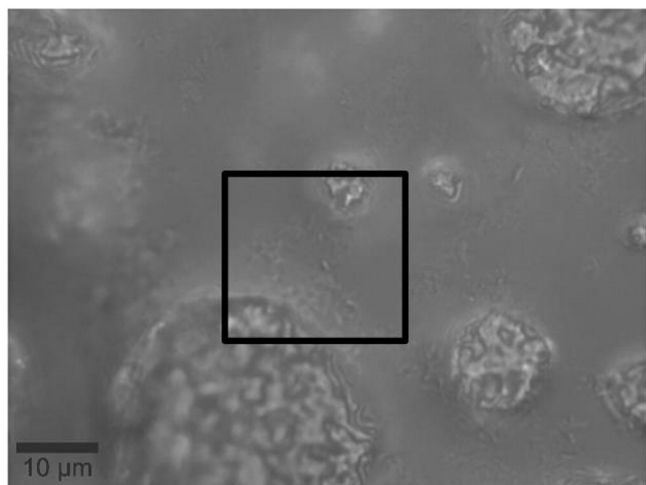


Fig. 8. Optical image of the sample (10 wt.% MDG) under white light illumination. The surface of the air cells is wrinkled as a result of the adsorption of fat crystals. The frame (20 μm × 20 μm) indicates the area of the Raman mapping.

approximately 100 ml of foam was turned upside-down and the image of Supporting information 2 provides clear evidence that the material did not flow. Instead, it behaved like a strong gel that sustained its own weight without any apparent deformation. The gravity stress that

acts on the air bubbles can be estimated considering the ratio between the buoyancy force, P_b , and the equatorial section of the bubbles:

$$\tau_b = \frac{P_b}{\pi \langle r \rangle^2} \approx \frac{4}{3} \langle r \rangle \rho_{oil} g \quad (5)$$

where g is the earth gravity constant and ρ_{oil} is the oil density. Taking $\langle r \rangle = 50 \mu\text{m}$, we obtain $\tau_b \approx 0.7 \text{ Pa}$, which is far below the yield stress values, τ_v , reported in Table 2. This explains why bubbles are not submitted to segregation phenomena over time.

During the whipping process, air is incorporated either via the random agitation exerted by a whisk or through the forced injection of gas into a liquid submitted to shear. The application of a spatially homogeneous shear without incorporating air generally provokes foam destruction. For example, this is the case for whipped dairy creams. We probed the shear resistance of the oil foams by processing them in the Couette's cell at a shear rate of 1000 s^{-1} . Surprisingly, the foams did not undergo destabilization and the air fraction remained at the same level as in the initial conditions, i.e. close to 55 vol.%. The resulting structure was observed under the microscope (see Supporting information 3). The applied shear has the effect to provoke a nearly 2-fold decrease in the average bubble size. The viscous stress applied under simple shear conditions has thus provoked break-up of mother bubbles into daughter ones with a smaller size. Higher shear rates were probed (up to $14\,500 \text{ s}^{-1}$) but the final bubble size did not decrease significantly, suggesting that bubble recombination also occurred. Overall, it can be stated that the obtained foams are processable and can resist flow

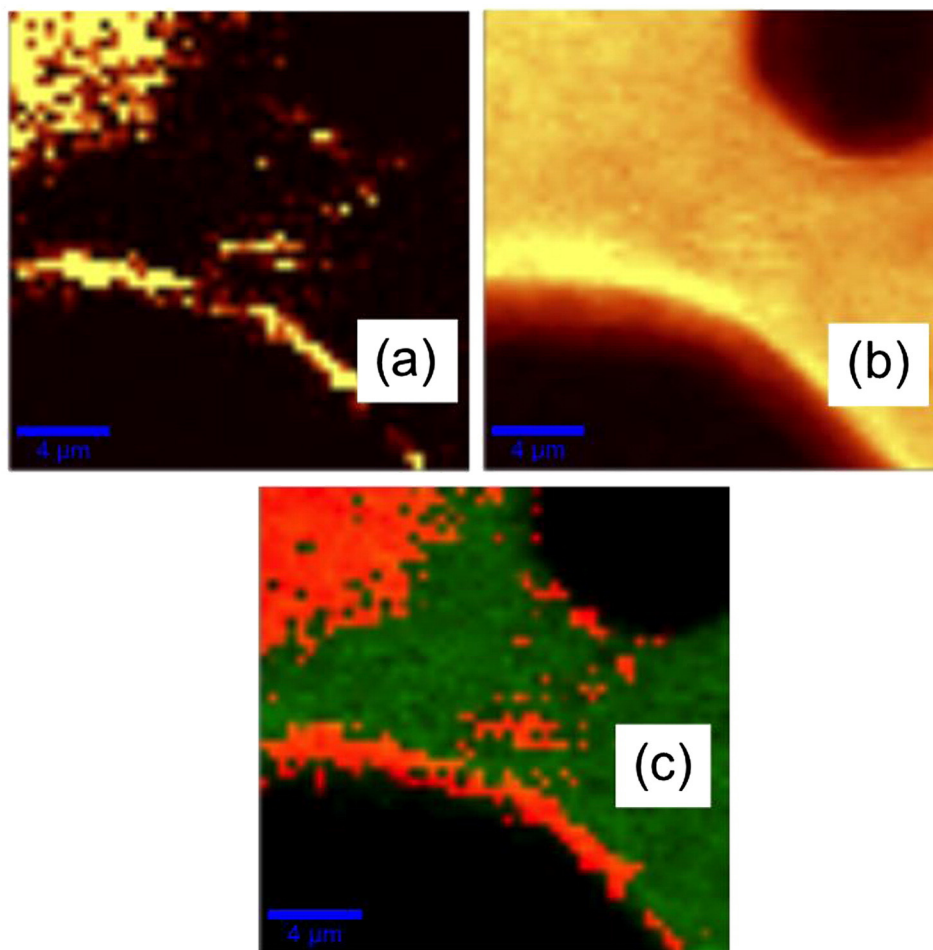


Fig. 9. Raman intensity images representing the localization of (a) MDG and of (b) oil; and (c): superposition of the previous images: red for MDG, green for oil and black for air bubbles. The scale bar represents 4 μm. (For interpretation of the references to color in this figure legend, the reader is referred to the web version of this article.)

Table 2
Rheological properties of the oil foams.

MDG content in the oil phase (wt.%)	G' (Pa)	G'' (Pa)	τ_v (Pa)
5.0	$(4.0 \pm 0.2) \times 10^3$	$(1.6 \pm 0.1) \times 10^3$	$(0.8 \pm 0.1) \times 10^2$
10.0	$(9.2 \pm 0.5) \times 10^3$	$(4.9 \pm 0.3) \times 10^3$	$(2.5 \pm 0.3) \times 10^2$
15.0	$(3.4 \pm 0.2) \times 10^4$	$(1.8 \pm 0.1) \times 10^4$	$(9.2 \pm 0.5) \times 10^2$
20.0	$(6.7 \pm 0.4) \times 10^4$	$(3.9 \pm 0.2) \times 10^4$	$(1.8 \pm 0.1) \times 10^3$

transport without air leakage, as required in many industrial processes. More importantly, the bubble size of the sheared foams remained constant at a time scale of at least 3 months.

3.3. Air-in-oil-in-water emulsions

The oil foams were emulsified in an aqueous phase with the aim of producing air-in-oil-in water emulsions. Such systems are composed of oil droplets dispersed in an external aqueous phase, with the oil phase containing smaller air bubbles.

Since the oil foams were highly viscous, a strong shear stress was needed during the emulsification step to facilitate oil droplet dispersion. The external aqueous phase was prepared by dissolving 10 wt.% gum arabic. Due to its amphiphilic properties, gum arabic facilitated break-up and further stabilization of the oil droplets in the external aqueous solution. In the first trials, 25 ml of oil foam and 25 ml of external aqueous phase were poured into a beaker. The two phases were then submitted to vigorous agitation by means of an Ultra-Turrax homogenizer (T25 Janke & Kunkel) equipped with a S25 KV-25 F rotor head, operating at 9000 rpm for 1 min. For $\phi_{MDG} \leq 10$ wt.%, emulsions were produced but the turbulent mixing resulted in a significant reduction of the total volume reflecting the almost full release of the air bubbles. This was checked by observing the samples under the microscope. The obtained emulsions were mainly composed of simple oil-in-water droplets and only a few droplets contained air bubbles. For $\phi_{MDG} \geq 15$ wt.%, large macroscopic clumps were formed probably reflecting partial coalescence of the oil droplets because of their high solid content. From these preliminary experiments, we conclude that mild conditions in terms of agitation are required during the emulsification step to fragment the oil phase into the aqueous one and to preserve the multiple structure. We thus adopted an alternative strategy based on the application of shear under laminar flow conditions in a highly viscous aqueous phase.

For droplet deformation to occur, the applied shear stress, $\eta_c \dot{\gamma}$, where η_c is the viscosity of the continuous phase and $\dot{\gamma}$ is the applied shear rate, must overcome the characteristic Laplace pressure of the droplets, $4\sigma/d$, where σ is the oil/water interfacial tension and d is the droplet diameter (Mabille et al., 2000 and references therein). For rupturing to occur, the capillary number defined as the ratio of the applied stress to half of the Laplace pressure, $C_a = \eta_c \dot{\gamma} d / 2\sigma$, must exceed a critical value C_{ac} . This implies that the droplet has been elongated by the viscous shear before rupturing. The average droplet diameter of the ruptured droplets is thus given by:

$$d = \frac{2C_{ac}\sigma}{\eta_c \dot{\gamma}} \quad (6)$$

The parameter C_{ac} depends on the type of shear flow (simple shear or elongational) and on the continuous-to-dispersed phase viscosity ratio (Mabille et al., 2000; and references therein). Following Eq. (6), in order to fragment the droplets at low shear rates, a relatively large viscosity of the continuous phase is needed. In our experiments, this was achieved by dissolving a thickening agent, namely xanthan, in the aqueous phase.

The primary oil foam was sheared in the Couette's cell at 1000 s^{-1} and the average bubble size was close to $25 \mu\text{m}$. This foam was then progressively dispersed in an aqueous phase containing 10 wt.% gum arabic, 3 wt.% xanthan and 0.02 wt.% sodium azide under gentle manual stirring by means of a spatula, at room temperature. The obtained coarse dispersion was finally sheared in the Couette's cell to reduce the droplet size. Fig. 10 shows microscope images of an emulsion based on 10 wt.% MDG in the oil phase. Only 5 vol.% of oil foam was emulsified in the external aqueous phase in order to easily discern the A/O/W structure. The 3 images were obtained at different shear rates: (a) 2100 s^{-1} ;

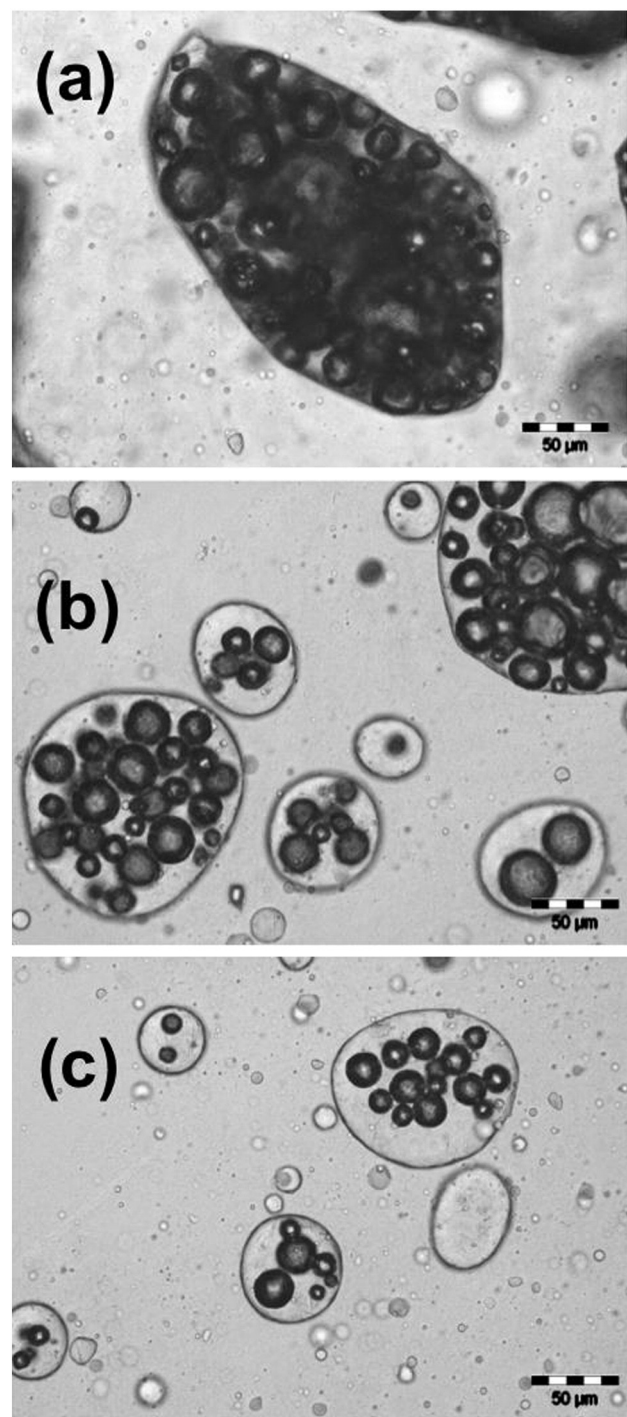


Fig. 10. Microscope images of an emulsion of the A/O/W type. The oil phase contains 10 wt.% MDG and the aqueous phase comprises 10 wt.% gum arabic and 3 wt.% xanthan. The emulsion was sheared in the Couette's cell at: (a) 2100 s^{-1} ; (b) 6300 s^{-1} ; and (c) 10500 s^{-1} . The scale bar represents $50 \mu\text{m}$.

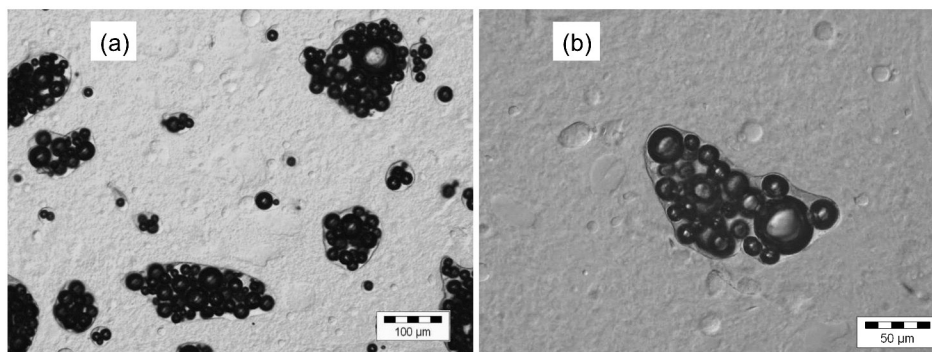


Fig. 11. Microscope images of an emulsion of the A/O/W type. The oil phase contains 10 wt.% MDG and the aqueous phase comprises 5 wt.% sodium caseinate and 1 wt.% hydroxyethyl cellulose. The emulsion was sheared in the Couette's cell at 2000 s^{-1} .

(b) 6300 s^{-1} ; and (c) $10\,500 \text{ s}^{-1}$. The oil droplets are irregularly shaped because of their intrinsic firmness that did not allow full shape relaxation once the applied shear was stopped. The oil droplets contain air bubbles with the same characteristic size as in the primary foam. The oil envelope surrounding air bubbles is clearly visible, especially in frames (b) and (c). More importantly, the images in Fig. 10 reveal some trends as the applied shear rates increases: both the average droplet size and the fraction of encapsulated air bubbles decrease. This means that the shear rate must be optimized: the applied shear has to be large enough to produce droplet break-up but low enough to avoid the release of the air bubbles. The decrease of the air fraction in the oil droplets at high shear rates is most probably reflecting coalescence phenomena of the bubbles on the droplet surface. The same phenomenology has been observed in water-in-oil-in-water (W/O/W) double emulsions submitted to high shear. Muguet et al. (1999) showed that there is a correlation between the inner aqueous droplet release and oil droplet fragmentation. Indeed, they observed that coalescence-driven release of the inner droplets occurred always in conjunction with oil droplet fragmentation.

To check the generality of our findings we probed other combinations of surface-active species and thickening agents in the aqueous external phase. For example, Fig. 11 shows two images of an A/O/W emulsion sheared at 2000 s^{-1} whose continuous phase contained 5 wt.% sodium caseinate (emulsifier) and 1 wt.% hydroxyethyl cellulose (thickener). The images show the same features as those reported in Fig. 10, the average diameters of the air bubbles and of the oil droplets being of the order of several tens of micrometers and several hundreds of micrometers, respectively. An emulsion containing 50 vol.% oil foam was fabricated at 2000 s^{-1} following the same process and using the same components. To check that air was actually present in the system at the expected content, the emulsion was submitted to intense centrifugation at 3000 g for 2 h. The photos of Supporting information 4 illustrate the macroscopic state of the system. In its initial state, the emulsion (SI 4-a) is macroscopically homogeneous and milky. After centrifugation, the emulsion is ruptured with the aqueous phase residing at the bottom of the centrifuge tube (SI 4-b). The upper part of the sample is a remnant of the oil foam and is composed of 3 layers. The bottom layer contains MDG crystals which are denser than rapeseed oil. The middle layer is transparent and mostly contains rapeseed oil. The top layer is a concentrated stack of air bubbles which have withstood the buoyant stress. Interestingly, centrifugation has provoked a release of a large fraction of air bubbles, as evidenced by the large volume variation. For the sake of comparison, the arrow in SI 4-b indicates the initial level of emptying of the centrifuge tube. Full release of the air bubbles was obtained after 5-hour centrifugation and within experimental uncertainty, the volume decrease was equivalent to $\sim 25\%$, very close to the expected value ($\sim 27.5\%$) considering the initial overrun of the oil foam ($\sim 55\%$).

The colloidal structure of the A/O/W droplets was preserved after one-month storage at room temperature. Up to our knowledge, this is the first proof of concept for the fabrication of A/O/W emulsions. These materials offer the unique advantage of reconciling large fractions of dispersed phase with relatively low fat content. Such formulation strategy can thus be used for the production of low caloric texturized products.

4. Conclusion

In this paper, we prepared the foams by incorporating air bubbles in a vegetable oil/MDG mixture. We probed the kinetic stability of the foams under various conditions. All systems under study exhibited outstanding stability both at rest and under shear. We demonstrated that the air bubbles are stabilized against coalescence and Ostwald ripening by a dense layer of surfactant crystals. Concomitantly, the excess surfactant in the oil phase forms a rigid network whose intrinsic firmness hinders buoyancy driven segregative phenomena. The obtained foams are reminiscent of Pickering emulsions stabilized by solid particles (Leal-Calderon & Schmitt, 2008). The stability of the obtained foams under shear is rather unusual and allowed us to reduce the bubble size by processing the foam in a Couette's cell device at sufficiently high shear rates. Interestingly, the foams were stimulus responsive, as they could be destabilized by raising the temperature above the melting range of the MDG surfactant mixture. Finally, we prepared a new type of material, namely air-in-oil-in-water (A/O/W) emulsions by dispersing the oil foams in an aqueous phase containing hydrophilic surface-active species and thickening hydrocolloids.

It is within the reach of future work to reduce the amount of MDG in the formulations by substituting them by crystallizable triglycerides. MDG crystals may act as nuclei to induce triglyceride crystallization, allowing the formation of a firm crystal network that identically stabilize oil foams. In parallel, reducing the size of the air bubbles poses a real challenge. On the one hand, this could lead to foams with novel textural properties. On the other hand, smaller bubbles could facilitate the fabrication of A/O/W emulsions with much finer droplets than the ones achieved in the present paper.

Acknowledgments

The authors gratefully acknowledge the Aquitaine Regional Council for financial support.

Appendix A. Supplementary data

Supplementary data to this article can be found online at <http://dx.doi.org/10.1016/j.foodres.2014.11.044>.

References

- Alargova, R.G., Warhadpande, D.S., Paunov, V.N., & Velev, O.D. (2004). Foam superstabilization by polymer microrods. *Langmuir*, 20, 10371–10374.
- Arditty, S., Schmitt, V., & Leal-Calderon, F. (2005). Interfacial properties in solid-stabilized emulsions. *European Physical Journal B*, 44, 381–393.
- Battino, R., Rettich, T.R., & Tominaga, T. (1984). The solubility of nitrogen and air in liquids. *Journal of Physical and Chemical Reference Data*, 13, 563–600.
- Binks, B.P., & Horozov, T.S. (2005). Aqueous foams stabilized solely by silica nanoparticles. *Angewandte Chemie International Edition*, 44, 3722–3725.
- Binks, B.P., Rocher, A., & Kirkland, M. (2011). Oil foams stabilized solely by particles. *Soft Matter*, 7, 1800–1808.
- Binks, B.P., Sekine, T., & Tyowua, A.T. (2014). Dry oil powders and oil foams stabilized by fluorinated clay platelet particles. *Soft Matter*, 10, 578–589.
- Durian, D.J., Weitz, D.A., & Pine, D.J. (1991). Multiple light-scattering probes of foam structure and dynamics. *Science*, 252, 686–688.
- Exerowa, D., & Kruglyakov, P.M. (1998). *Foams and foam films*. Amsterdam: Elsevier.
- Friberg, S.E., & Ahmad, S.I. (1971). Liquid crystals and the foaming capacity of an amine dissolved in water and *p*-xylene. *Journal of Colloid and Interface Science*, 35, 175.
- Friberg, S.E., Blute, I., Kunieda, H., & Stenius, P. (1986). Stability of hydrophobic foams. *Langmuir*, 2, 659–664.
- Friberg, S.E., Chang, S., Green, W.B., & Gilder, R.V. (1984). A nonaqueous foam with excellent stability. *Journal of Colloid and Interface Science*, 101, 593–595.
- Fujii, S., Ryan, A.J., & Armes, S.P. (2006). Long-range structural order, moiré patterns, and iridescence in latex-stabilized foams. *Journal of the American Chemical Society*, 128, 7882–7886.
- Hotrum, N.E., Cohen-Stuart, M.A., van Vliet, T., & van Aken, G.A. (2004). Spreading of partially crystallized oil droplets on an air/water interface. *Colloids and Surfaces A*, 240, 83–92.
- Kunieda, H., Shrestha, L.K., Acharya, D.P., Kato, H., Takase, Y., & Gutierrez, J.M. (2007). Super-stable nonaqueous foams in diglycerol fatty acid esters-non polar oil systems. *Journal of Dispersion Science and Technology*, 28, 133–142.
- Leal-Calderon, F., & Schmitt, V. (2008). Solid-stabilized emulsions. *Current Opinion in Colloid and Interface Science*, 13, 217–227.
- Lemlich, R. (1978). Prediction of changes in bubble-size distribution due to interbubble gas diffusion in foam. *Industrial and Engineering Chemistry Fundamentals*, 17, 89–93.
- Lifshitz, I.M., & Slyozov, V.V. (1961). The kinetics of precipitation from supersaturated solid solutions. *Journal of Physics and Chemistry of Solids*, 19, 35–50.
- Mabille, C., Schmitt, V., Gorria, P., Leal-Calderon, F., Faye, V., Deminière, B., et al. (2000). Rheological and shearing conditions for the preparation of monodisperse emulsions. *Langmuir*, 16, 422–429.
- Morrison, I.D., & Ross, S. (2002). *Colloidal dispersions: Suspensions, emulsion and foams*. New York: Wiley & Sons, Inc.
- Muguet, V., Seiller, M., Barratt, G., Clausse, D., Marty, J.P., & Grossiord, J.L. (1999). W/O/W multiple emulsions submitted to a linear shear flow: Correlation between fragmentation and release. *Journal of Colloid and Interface Science*, 218, 335–337.
- Prud'homme, R.K., & Khan, S.A. (1996). *Foams: Theory, measurements, and applications*. New York: Marcel Dekker, Inc.
- Shrestha, L.K., Aramaki, K., Kato, H., Takase, Y., & Kunieda, H. (2006). Foaming properties of monoglycerol fatty acid esters in nonpolar oil systems. *Langmuir*, 22, 8337–8345.
- Shrestha, L.K., Kaneko, M., Sato, T., Acharya, D.P., Iwanaga, T., & Kunieda, H. (2006). Phase behavior of diglycerol fatty acid esters–nonpolar oil systems. *Langmuir*, 22, 1449–1454.
- Shrestha, L.K., Sato, T., Acharya, D.P., Iwanaga, T.K., & Kunieda, H.J. (2006). Phase behavior of monoglycerol fatty acid esters in nonpolar oils: Reverse rodlike micelles at elevated temperatures. *Physical Chemistry B*, 110, 12266–12273.
- Shrestha, L.K., Shrestha, R.G., Sharma, S.C., & Aramaki, K. (2008). Stabilization of nonaqueous foam with lamellar liquid crystal particles in diglycerol monolaurate/olive oil system. *Journal of Colloid and Interface Science*, 328, 172–179.
- Shrestha, R.G., Shrestha, L.K., Solans, C., Gonzalez, C., & Aramaki, K. (2010). Nonaqueous foam with outstanding stability in diglycerol monomyristate/olive oil system. *Colloids and Surfaces A*, 353, 157–165.
- Subramaniam, A.B., Mejean, C., Abkarian, M., & Stone, H.A. (2006). Microstructure, morphology, and lifetime of armored bubbles exposed to surfactants. *Langmuir*, 22, 5986–5990.
- Wagner, C. (1961). Theorie der alterung von niederschlägen durch umlösen (Ostwald Reifung). *Zeitschrift für Elektrochemie*, 65, 581–591.
- Walstra, P., Kloek, W., & van Vliet, T. (2001). Fat crystals networks. In K. Sato, & N. Garti (Eds.), *Crystallization processes in fats and lipid systems* (pp. 289–328). New York: Marcel Dekker.
- Yuqing Zhou, Y., & Hartel, R. (2006). Phase behavior of model lipid systems: Solubility of high-melting fats in low-melting fats. *Journal of the American Oil Chemists' Society*, 83, 505–511.